

$1/T_1$ in the D-wave superconducting state with coexisting antiferromagnetism

Yunkyu Bang*, M. J. Graf, A.V. Balatsky, and J. D. Thompson
Los Alamos National Laboratory, Los Alamos, New Mexico 87545
(May 25, 2020)

We consider a general D-wave superconducting gap function in the presence of coexisting antiferromagnetic (AFM) long-range order. We find that the D-wave order parameter develops additional nodes without lowering the symmetry of the state due to the interplay of the superconducting and AFM correlations. This AFM correlated D-wave gap has a small gap structure inside the generic D-wave gap. As a result of this additional structure it shows a quite different response to impurities compared to a standard D-wave gap. We calculate the nuclear spin-lattice relaxation rate $1/T_1$ of this gap in the presence of impurities and discuss the implications for the experiments of some AFM heavy-fermion superconductors and in particular for CeRhIn₅.

PACS numbers: 74.20, 74.20-z, 74.50

I. INTRODUCTION

The interplay and competition between antiferromagnetism (AFM) and superconductivity (SC) is a long studied subject both experimentally¹ and theoretically². There are now several heavy fermion compounds showing clear experimental evidence of the microscopically homogeneous coexistence of AFM and SC correlations³⁻⁶. However, the direct consequences of the coexistence of AFM and SC has not yet been clearly resolved. Recent ¹¹⁵In- NQR studies of CeRhIn₅ and CeIn₅ also revealed that there is a coexistence region of AFM and SC around the critical pressures of 1.6 GPa and 2.43 GPa, respectively⁷. Apart from confirming the coexistence of AFM and SC in this region of pressure, an interesting observation is that the nuclear spin-lattice relaxation rate $1/T_1$ displays the linear temperature dependence $1/T_1 \propto T$ at low temperatures (up to $0.3 T_{sc}$ for CeRhIn₅), followed by the T^3 behavior below the superconducting transition temperature T_{sc} . The latter behavior is an indication of the lines of nodes of the anisotropic SC state.

The standard explanation of the T-linear temperature dependence of $1/T_1$ at low temperatures is the impurity effect in an unconventional SC with lines of nodes. However, this impurity explanation has difficulties in the case of CeRhIn₅; the low temperature T-linear $1/T_1$ is only observed in the AFM and SC coexistence region at 1.6 GPa, and once the AFM order disappears by increasing pressure to 2.1 GPa, $1/T_1$ exhibits a T^3 behavior for the entire measured temperatures below T_{sc} ⁸. Similar pressure dependence of $1/T_1$ has also been observed in Ge-substituted CeCu₂Si₂⁵. Another AFM heavy fermion superconductor URu₂Si₂⁴ also shows the low temperature T-linear behavior in $1/T_1$. In the case of UPd₂Al₃, the situation is somewhat different; a more recent NMR experiment⁶ indicates that the T-linear behavior observed in earlier experiments disappears with purer samples. Putting together these observations we think that the interplay of the AFM and SC, together with some sort of impurity effects, should hold the key to explain

the $1/T_1 \propto T$ behavior at low temperatures in these AFM heavy fermion superconductors. In particular, we think this is the case for CeRhIn₅ under pressure, where at low temperatures $1/T_1 \propto T$ is observed in the coexistence region (P=1.6 GPa), but is replaced by $1/T_1 \propto T^3$ once the AFM is suppressed (P=2.1GPa).

There is a substantial body of studies on the interplay/coexistence between D-wave SC and AFM². The general conclusion of these studies is that, depending on the parameters in the model, these two phases either exclude each other or can coexist together. Here, however, we are motivated by the above-mentioned magnetic heavy-fermion (HF) superconducting materials, where the Néel temperature T_N usually sets in first at a higher temperature and then at a lower temperature the SC transition occurs on top of the AFM ordering. Henceforth, we assume the coexistence of D-wave SC and AFM and confine our interest on how a general D-wave SC order parameter (OP) should be modified due to the presence of the AFM long range order. We found an important modification of the D-wave gap due to the long range AFM order; the D-wave SC state develops additional nodes in the gap function that are a direct consequence of the crossing between the Fermi surface (FS) and the magnetic Brillouin zone (BZ), see Fig.1. At these discrete crossing points the superconducting order parameter is forced to vanish by the AFM coherence factors⁹. These additional nodes (we call them *AFM nodal points*) lead to a density of states (DOS), which is almost gapless down to very low energy before it develops a steeply decreasing DOS, see Fig.2. This shape of the DOS is intrinsically vulnerable to a small amount of impurities, which fill rapidly the small gap and produce a large finite DOS.

From this AFM+D-wave gap solution we calculate the nuclear spin-lattice relaxation rate $1/T_1$ in the presence of impurities. We find that the response of this AFM+D-wave gap to impurities is quite different from the one of the standard D-wave gap. The main findings are: (1) the AFM+D-wave gap produces more quickly a finite DOS at $\omega = 0$ than the standard D-wave gap, both for Born and

for unitary impurity scattering, (2) for unitary scattering, the calculated $1/T_1$, both for the AFM+D-wave gap and for the standard D-wave gap, produces the T-linear behavior at very low temperatures. The temperature regions of T-linear behavior are about the same for both gaps with the same amount of impurity concentration despite the different low energy behaviors of the DOS. However, the magnitude of $1/T_1$ in the T-linear region is about 4 times smaller for the standard D-wave gap than for the AFM+D-wave gap, (3) for Born limit scattering, the $1/T_1$ of the AFM+D-wave gap can still produce the T-linear behavior in a substantial region of low temperatures but with a much higher impurity concentration than with unitary impurities. In order to achieve the same T-linear behavior as for unitary scattering, about 5 times the amount of impurity concentration is needed. On the other hand, the standard D-wave gap hardly shows any T-linear behavior with the same amount of impurities, but displays almost T^3 power law for the entire temperature range below T_{sc} with a small deviation due to impurities.

Considering the experimental observation of the T-linear behavior in $1/T_1$ in some of the AFM heavy fermion superconductors, we propose that the AFM+D-wave gap structure together with Born limit impurities can be the reason for the T-linear behavior in $1/T_1$ in these compounds. When the AFM long range order disappears by tuning pressure in CeRhIn₅, as well as in CeCu₂(Si_{0.98}Ge_{0.02})₂, the SC gap gradually returns to a standard D-wave gap and then a small amount of Born scatterers is not enough to produce the T-linear $1/T_1$ ^{5,7}. One remaining question of this scenario is the possible source of the Born limit scatterers. We think that the most probable source of scatterers in the Born limit is strain in the lattice induced with pressure and/or AFM domain walls in CeRhIn₅ and through chemical substitution in CeCu₂(Si_{0.98}Ge_{0.02})₂⁵.

II. FORMALISM

The Hamiltonian describing the coexistence of AFM and SC pairing interactions is written as

$$H = \sum_{k,\sigma} [\epsilon_k c_{k,\sigma}^\dagger c_{k,\sigma} + \sigma \Delta_M c_{k+Q,\sigma}^\dagger c_{k,\sigma}] + \sum_{k,k'} V(k,k') c_{k,\sigma}^\dagger c_{-k,\sigma'}^\dagger c_{-k',\sigma'} c_{k',\sigma}, \quad (1)$$

where we replaced the AFM pairing interaction by its mean-field AFM OP Δ_M . In the presence of the AFM order, the conduction band is split into two AFM quasiparticle bands:

$$\begin{aligned} \alpha_{(1),\sigma,k} &= u_k c_{\sigma,k} - \sigma v_k c_{\sigma,k+Q}, \\ \alpha_{(2),\sigma,k} &= \sigma v_k c_{\sigma,k} + u_k c_{\sigma,k+Q}, \end{aligned} \quad (2)$$

with the AFM Bogoliubov coefficients, $u_k^2 = 1/2 + \frac{\delta_k}{2\sqrt{\delta_k^2 + \Delta_M^2}}$, and $v_k^2 = 1/2 - \frac{\delta_k}{2\sqrt{\delta_k^2 + \Delta_M^2}}$. The quasiparticle energy and the convenient parameters are defined as

$$E_{(1),(2)} = \zeta_k \pm \sqrt{\delta_k^2 + \Delta_M^2}, \quad (3)$$

$$\zeta_k = \frac{1}{2}[\epsilon_k + \epsilon_{k+Q}], \quad (4)$$

$$\delta_k = \frac{1}{2}[\epsilon_k - \epsilon_{k+Q}]. \quad (5)$$

Then the original SC pairing interaction is rewritten in terms of the AFM quasiparticle wave function,

$$\begin{aligned} H_{int} &= \sum_{k,k'} V(k,k') c_{\uparrow,k}^\dagger c_{\downarrow,-k}^\dagger c_{\downarrow,-k'} c_{\uparrow,k'} \\ &= \sum_{k,k'} V(k,k') (u_k^2 - v_k^2) \alpha_{(2)\uparrow,k}^\dagger \alpha_{(2)\downarrow,-k} \\ &\quad \alpha_{(2)\downarrow,-k'} \alpha_{(2)\uparrow,k'} (u_{k'}^2 - v_{k'}^2) + \dots, \end{aligned} \quad (6)$$

where the ellipsis stands for terms like $\alpha_1^\dagger \alpha_1 \alpha_1^\dagger \alpha_1$ and all the mixed terms of α_1 and α_2 . In this approximation we certainly keep the pairing term in the lower AFM quasiparticle band assuming that the Fermi level crosses the lower band and that the AFM gap Δ_M is much larger than the SC gap Δ_{sc} . This approximation should apply for the case $T_N \gg T_{sc}$. Then the singlet gap equation is written as

$$\begin{aligned} \Delta_\alpha(k) &= (u_k^2 - v_k^2) \sum_{k'} V(k,k') < \alpha_{(2)\uparrow,k'} \alpha_{(2)\downarrow,-k'} > \\ &\quad \times (u_{k'}^2 - v_{k'}^2). \end{aligned} \quad (7)$$

This gap equation was obtained by Buzdin and Bulaevskii⁹ for s-wave SC. The important point is that the AFM coherence factor $(u_k^2 - v_k^2)$ modifies the otherwise standard D-wave gap equation where SC is mediated by the pairing potential $V(k,k')$. At those points where $(u_k^2 - v_k^2) = 0$ is satisfied, the gap function $\Delta_\alpha(k)$ should vanish in addition to the D-wave nodal points. Now for simplicity of numerical calculations, we assume a circular FS in two dimensions and the gap equation is generalized to account for impurity effects¹⁰. The effect of the impurity scattering is included with T-matrix approximation¹¹. For the particle-hole symmetric case $T_3 = 0$, and for D-wave OP with isotropic scattering $T_1 = 0$ (also without loss of generality we can choose $T_2 = 0$ by U(1) symmetry). Then we need to calculate only $T_0(\omega)$. The impurity selfenergy is given by $\Sigma_0 = \Gamma T_0$, where $\Gamma = n_i/\pi N_0$, N_0 is the normal DOS at the Fermi energy, n_i is the impurity concentration; $T_0(\omega_n) = \frac{g_0(\omega_n)}{[c^2 - g_0^2(\omega_n)]}$, where $g_0(\omega_n) = \frac{1}{\pi N_0} \sum_k \frac{i\tilde{\omega}_n}{\tilde{\omega}_n^2 + \epsilon_k^2 + \Delta^2(k)}$, $\tilde{\omega}_n = \omega_n + \Sigma_0$ ($\omega_n = \pi T(2n+1)$), and the scattering strength parameter c is related to the s-wave phase shift δ by $c = \cot(\delta)$. With this T_0 the following gap equation is solved self-consistently.

$$\Delta(\phi) = -N(0) \cdot g(\phi) \int \frac{d\phi'}{2\pi} V(\phi - \phi') \\ \times T \sum_{\omega_n} \int_{-\omega_D}^{\omega_D} d\epsilon \frac{\Delta(\phi')}{\tilde{\omega}_n^2 + E_{(2)}^2(\epsilon) + \Delta^2(\phi')} \cdot g(\phi'), \quad (8)$$

where $g(\phi)$ is the angular parametrization of $(u_k^2 - v_k^2)$. In contrast to previous works on the D-wave SC, where the form of the D-wave SC gap has a fixed functional form such as $\Delta(\vec{k}) = \Delta_0(\cos k_x - \cos k_y)$ or $\cos(2\phi)$, we allow for a most general D-wave OP of D_2 symmetry; namely $\Delta(n\pi/4) = 0$ ($n = 1, 3, 5, 7$), $\Delta(\phi) = \Delta(\phi \pm \pi)$, and $\Delta(\phi) = -\Delta(\phi \pm \pi/2)$. Therefore the gap equation can produce the most general D-wave symmetry gap solution for a given pairing potential and now with an additional constraint from the AFM correlation. The pairing potential $V(\phi - \phi')$ induces a D-wave gap. Although its microscopic origin is not an issue in this paper, we believe it originates from AFM fluctuations. The static limit of AFM fluctuations $\chi(\mathbf{q}, \omega = 0) \sim \frac{1}{(q-Q)^2 + \xi^{-2}}$ is parameterized as^{10,12}

$$V(\phi - \phi') = V_a(b) \frac{b^2}{(\phi - \phi' \pm \pi/2)^2 + b^2} \quad (9)$$

where the parameter b is proportional to ξ^{-1} , normalized in the circular FS ($\xi \sim a\pi/b$; a is the lattice parameter). For all calculations in this paper, we choose $b = 0.5$ which is not a sensitive parameter for our results.

With the gap function $\Delta(\phi)$ and $T_0(\omega)$ obtained from Eq.(8) ($T_0(\omega)$ is analytically continued from $T_0(\omega_n)$ by Padé approximant method), we calculate the $1/T_1$ nuclear spin-lattice relaxation rate^{11,13}

$$\frac{1}{T_1 T} \sim \int_0^\infty \frac{\partial f_F(\omega)}{\partial \omega} [(\langle \text{Re} \frac{\tilde{\omega}}{\sqrt{\tilde{\omega}^2 - \Delta^2(\phi)}} \rangle_\phi)^2 \\ + (\langle \text{Re} \frac{\Delta(\phi)}{\sqrt{\tilde{\omega}^2 - \Delta^2(\phi)}} \rangle_\phi)^2], \quad (10)$$

where $\tilde{\omega} = \omega + \Sigma_0(\omega)$ and $\langle \dots \rangle_\phi$ means the angular average over the FS. The first term in the bracket of Eq. (10) is $N^2(\omega)$. The second term vanishes in our calculations because of the symmetry of the OP. To calculate $1/T_1 T$ using Eq. (10), we need the full temperature dependent gap function $\Delta(\phi, T)$ and T_{sc} . Our gap equation Eq. (8) is basically the BCS gap equation, therefore it gives the BCS temperature behavior for $\Delta(\phi, T)$ and $\Delta_0/T_{sc} = 2.14$ for the standard D-wave SC. In order to account for strong coupling effects and a stronger anisotropy of our general D-wave gap solution, we use the phenomenological formula, $\Delta(\phi, T) = \Delta(\phi, T=0) \Xi(T)$ with $\Xi(T) = \tanh(\beta \sqrt{T_{sc}/T - 1})$, and parameters β and Δ_0/T_{sc} . Then we only need to calculate $\Delta(\phi, 0)$ at zero temperature. The temperature dependence of $\Sigma_0(\omega, T)$ ($= \Gamma T_0(\omega, T)$) is similarly extrapolated: $T_0(\omega, T) = T_0(\omega, T=0) \Xi(T) + T_{normal}(1 - \Xi(T))$, where $T_{normal} = \Gamma/(c^2 + 1)$ is the normal state T_0 . In our

numerical calculation $\beta = 1.74$ is fixed because this parameter is not sensitive for the final results. But the ratio Δ_0/T_{sc} is an important parameter to simulate strong coupling effects; the larger this ratio is the more the strong coupling effect is accounted for.

III. RESULTS AND DISCUSSIONS

Now let us discuss the numerical results. In Fig. (1) the schematic FS and the magnetic BZ are shown together with the two-dimensional original BZ. The points where the magnetic BZ and the original FS cross and therefore the condition $(u_k^2 - v_k^2) = 0$ is satisfied, are marked as *AFM nodal points*. The gap function vanishes at those points; in real space this means that the singlet SC pairing is prohibited along the (1,1) direction due to AFM spin correlations⁹. A schematic D-wave gap solution is drawn accordingly.

In Fig. (2), we show the normalized DOS $N(\omega)/N_0$ for two exemplary cases of the AFM nodal points ($\eta = 0.2$ and 0.4); the distance of the AFM nodal point from the D-wave nodal point is parameterized by $\eta = |\phi_{AFM} - \phi_D|/\phi_D$, where $\phi_D = \pi/4$ is the D-wave nodal point and ϕ_{AFM} is the AFM nodal point. The inset shows the corresponding gap solutions. We found empirically that $\Delta(\phi) \sim [\cos(2\phi) + 1.5 \eta \cos(6\phi)]$ is a very good approximation to fit the AFM+D-wave gap solutions. In real compounds, the distance of the AFM nodal points from the D-wave nodal points is determined by the shape of the original FS (before the AFM long range order is included). The key feature is that when the AFM nodal points are not very far from the D-wave nodal points, the DOS already develops the gapless feature (without impurities), except at very low energies. This very low energy region has a shallow gap (the steeply rising DOS region), which is intrinsically vulnerable to disorder.

Fig.3 (a) shows the DOS and $1/T_1$ calculated for the AFM+D-wave gap with unitary impurities ($c = 0$). The inset shows the normalized DOS of the AFM+D-wave gap solution with varying concentrations of the unitary scatterers. We choose $\eta = 0.3$ (see Fig. 2) for illustration of a typical AFM+D-wave gap. As explained above, the low energy region of the DOS is quickly filled with a small amount of impurities. With this choice of parameters the impurity scattering rate $\Gamma/\Delta_0 = 0.064$ is enough to completely fill the low energy gap region and $N(\omega = 0)$ reaches more than 50 % of the normal-state DOS N_0 . The main panel shows the nuclear spin-lattice relaxation rate $1/T_1$ in a log-log scale for the corresponding DOS in the inset. In Fig. 3 and Fig. 4 all $1/T_1$ results are normalized to $1/T_1=10$ at $T=T_{sc}$ for easy comparison. For the temperature dependence of the gap, we choose the parameters $\beta = 1.74$ and $\Delta_0/T_{sc} = 3$ for the AFM+D-wave gap to account for the strong coupling effects of superconductivity as explained before. As expected from the DOS results, due to the impurity induced residual states,

$1/T_1$ displays the linear-T dependence at low temperatures and the region of T-linear behavior increases with impurity concentration. For $\Gamma/\Delta_0 = 0.064$, this T-linear region extends up to $\sim 0.35 T_{sc}$. In the high temperature region, first of all, near T_{sc} the coherence peak is almost invisible because of the sign-changing gap function (the second term in Eq. (10) vanishes). Secondly, it shows the typical T^3 behavior below T_{sc} due to the lines of nodes in the gap until it goes through a gradual crossover region and finally to the T-linear region. The comparison with the experimental data of CeRhIn₅ at 1.6 GPa⁷ (green diamond symbols; the experimental data are normalized in the same fashion as the numerical results) is quite good with the theoretical calculation with $\Gamma/\Delta_0 = 0.064$. On the other hand, there is no way to fit the 2.1 GPa data (magenta diamonds) with any amount of impurities.

Fig.3 (b) shows the same calculations as in Fig.3 (a) for a standard harmonic D-wave ($\Delta(\phi) = \Delta_0 \cos(2\phi)$) for comparison. The parameters $\beta = 1.74$ and $\Delta_0/T_{sc} = 2.5$ are used for the harmonic D-wave case. Compared to the AFM+D-wave case, we notice the main difference in the DOS at low energies shown in the inset. The resonance feature of unitary scattering in the residual DOS $N(\omega \rightarrow 0)$ is seen more clearly but the value of $N(\omega = 0)$ is smaller than for the AFM+D-wave case (see Fig.3 (a)) with the same impurity scattering rate. As in the AFM+D-wave case, $1/T_1$ produces the T-linear behavior at low temperatures with impurities and the T^3 dependence at higher temperatures below T_{sc} . However, there are also some noticeable differences compared to the AFM+D-wave case. First, the T-linear region and the T^3 region are more clearly separated (a smaller crossover region compared to the AFM+D-wave gap case). This difference reflects the different shapes of the DOS for each case. Second, another more important difference is that the magnitude of the low temperature $1/T_1$ is about four times smaller for the harmonic D-wave than the one of the AFM+D-wave case with the same impurity concentration. Therefore, the comparison with the data of CeRhIn₅ at 1.6 GPa⁷ (green diamonds) shows a large deviation at low temperatures although the T-linear power law is reproduced. It is possible to fit the 1.6 GPa data with a much larger impurity scattering rate of $\Gamma/\Delta_0 \sim 0.16$ (not shown in Fig.3 (b) but which can be extrapolated from the shown results). On the other hand, in order to fit the 2.1 GPa data (magenta diamonds), Γ/Δ_0 needs to be 0.016 or smaller (see Fig.3 (b)). Thus, we would need an explanation for why the impurity scattering rate is suddenly reduced by more than one order of magnitude when changing pressure from 1.6 GPa to 2.1 GPa.

Summing up the results of our calculations for unitary impurity scattering, we found that both gap functions with unitary impurities have difficulties to explain consistently the experiments at 1.6 GPa and 2.1 GPa.

Now we consider the effects of Born impurity scattering. Fig.4 (a) shows the DOS and $1/T_1$ of the AFM+D-wave gap with Born limit impurities ($c = 1$). The inset

of Fig.4 (a) shows the DOS of the AFM+D-wave gap ($\eta = 0.3$) with different impurity concentrations. Compared to the unitary impurity case (Fig.3.(a)), the shape of the DOS looks almost the same except for the fact that the amount of impurity concentration needs to be about five times larger to achieve a similar residual DOS. As a result, $1/T_1$ looks similar as in the unitary impurity case (Fig.3 (a)) with five times larger impurity concentrations. We can fit the 1.6 GPa data of CeRhIn₅ with the Born impurity scattering rate $\Gamma/\Delta_0 = 0.32$.

However, the results for the harmonic D-wave gap with Born impurities are quite different. Fig.4 (b) shows the DOS and $1/T_1$ for the harmonic D-wave case with Born limit scatterers. With increasing impurity scattering rate up to $\Gamma/\Delta_0 = 0.32$, the zero frequency residual DOS $N(0)$ is less than 20% of N_0 . As a result $1/T_1$ never displays any noticeable T-linear behavior up to $\Gamma/\Delta_0 = 0.32$. On the other hand, the comparison with the 2.1 GPa data of CeRhIn₅^{7,8} shows that the experimental data can be fitted nicely with $\Gamma/\Delta_0 = 0.16$.

A consistent explanation of the experiments of CeRhIn₅ with our calculations is the following. We first estimate $\Delta_{0,2.1GPa}/\Delta_{0,1.6GPa} \sim 2$ from the experimental observation that $T_{sc;2.1GPa} \sim 2.3K$ and $T_{sc;1.6GPa} \sim 1 K$. Then at 1.6 GPa where the AFM and SC coexist, the SC gap function is the AFM+D-wave gap and we can fit the data with Born limit impurities of $\Gamma/\Delta_0 = 0.32$ (Fig.4 (a)). At 2.1 GPa where the AFM disappears, the SC gap becomes the standard harmonic D-wave gap. Assuming that the Born limit impurity concentration remains the same as in the 1.6 GPa sample, the effective impurity scattering rate reduces to $\Gamma/\Delta_0 = 0.16$, hence the data fits well again with our calculation (Fig.4 (b)).

The remaining question is the origin of the Born limit scatterers and its amount. We suggest it could be due to strain in the lattice induced with pressure and/or AFM domain walls in CeRhIn₅ and chemical substitution in CeCu₂(Si_{0.98}Ge_{0.02})₂. The scattering rate $\Gamma/\Delta_0 = 0.32$ in CeRhIn₅ at 1.6 GPa appears quite large. But considering $\Delta_0 \propto T_{sc} \sim 1 K$, this impurity scattering rate is actually quite possible even in the nominally clean sample. In fact, the measured specific heat coefficients at low temperatures ($C(T)/T$) both at 1.65 GPa and 2.1 GPa ($N_{1.65}(0)/N_{normal} \sim 0.4$ and $N_{2.1}(0)/N_{normal} \sim 0$)¹⁴ are consistent with our calculations of the residual DOS (see the insets of Fig.4 (a) and Fig.4 (b)).

IV. CONCLUSION

In summary, we considered the problem of the coexistence of AFM and D-wave SC. Assuming the case of $\Delta_{AFM} > \Delta_{SC}$, the gap equation is simplified and the AFM correlation imposes an additional constraint on the D-wave gap function. As a result we found an interesting modification of the D-wave gap function; the D-wave OP should develop additional nodes besides the original

D-wave nodes. The DOS of this AFM+D-wave gap solution has a generic feature of being almost gapless down to very low energy. This shape of the DOS is intrinsically vulnerable to a small amount of impurities to produce a final DOS having a large amount of gapless excitations.

We then calculated the nuclear spin-lattice relaxation rate $1/T_1$ with this AFM+D-wave gap solution as well as with a standard harmonic D-wave gap, and compared the results with the experimental $1/T_1$ of CeRhIn_5 ^{7,8}. We found that with unitary impurities both the AFM+D-wave gap and a standard harmonic D-wave gap can produce T-linear behavior in $1/T_1$ at low temperature with a small amount of unitary impurities. However, both models with unitary impurities cannot explain the 1.6 GPa and 2.1 GPa data together in a consistent way. Then with Born limit impurities, we could fit the CeRhIn_5 $1/T_1$ data at 1.6 GPa with the AFM+D-wave gap with the amount of impurities $\Gamma/\Delta_0 = 0.32$. Assuming that the gap function is changing from the AFM+D-wave form at 1.6 GPa to the standard D-wave form at 2.1 GPa, we could also fit the $1/T_1$ data at 2.1 GPa with the same amount of impurities. The success of our explanation of the $1/T_1$ nuclear spin-lattice relaxation rate of CeRhIn_5 with pressure supports the idea that a general D-wave gap function should develop additional nodal points besides the generic D-wave nodes in the region of coexisting AFM and D-wave SC. These additional nodes should be observable in carefully designed experiments probing the nodal quasiparticles¹⁵.

V. ACKNOWLEDGEMENT

We thank Prof. Y. Onuki, Prof. Kitaoka, Prof. Zheng, Dr. Kawasaki for providing the experimental data and discussions and are grateful to Dr. L.H. Bulaevskii for discussions. This work was supported by US DoE. Y.B. was partially supported by the Korean Science and Engineering Foundation (KOSEF) through the Center for Strongly Correlated Materials Research (CSCMR) (2002) and through the Grant No. 1999-2-114-005-5.

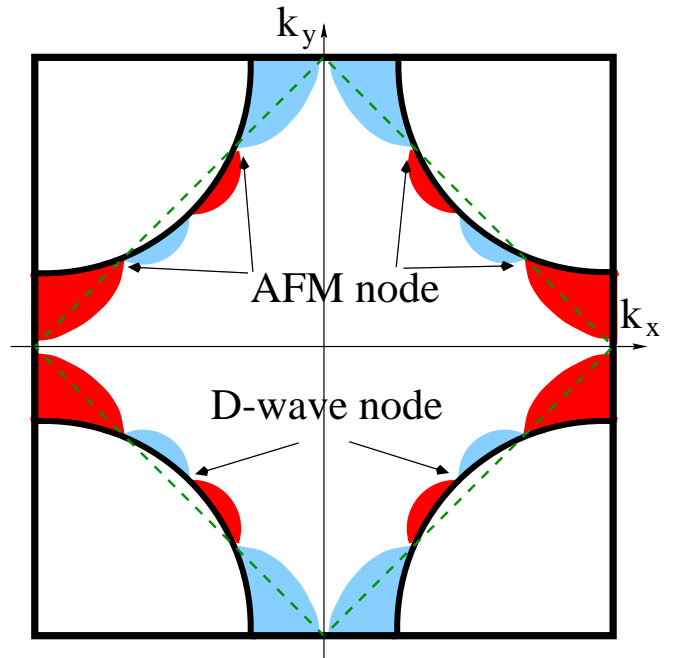


FIG. 1. The schematic magnetic Brillouin zone (BZ) (dashed line) and the Fermi surface (FS) in the two-dimensional BZ. The crossing points of the magnetic BZ and FS are the AFM nodal points. Also shown is the schematic gap solution of the AFM+D-wave gap equation (The red and blue colors indicate the sign-changing OP).

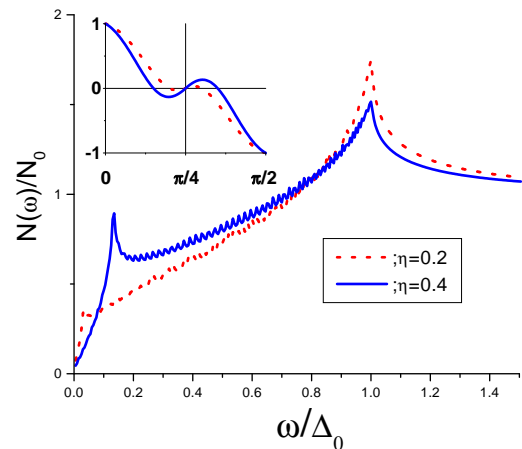


FIG. 2. The normalized DOS $N(\omega)/N_0$ for different positions of the AFM nodal points ϕ_{AFM} ; the red dotted line is for $\eta = |\phi_{AFM} - \phi_D|/\phi_D = 0.2$ and the blue solid line is for $\eta = 0.4$. Inset: The corresponding gap functions $\Delta(\phi)$.

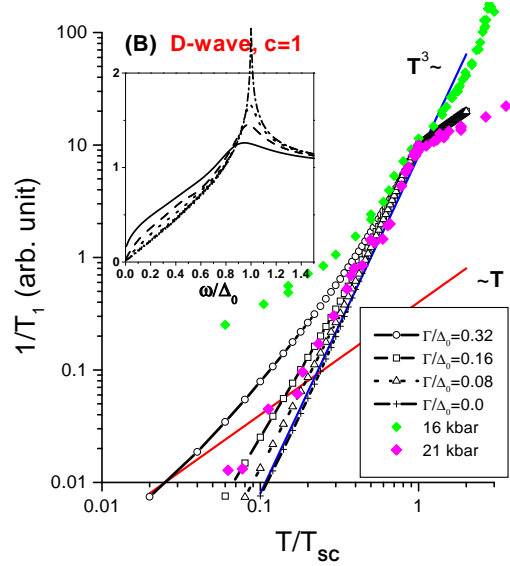
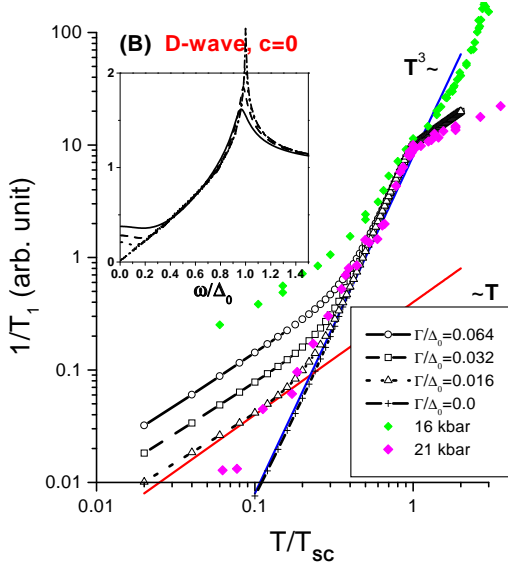
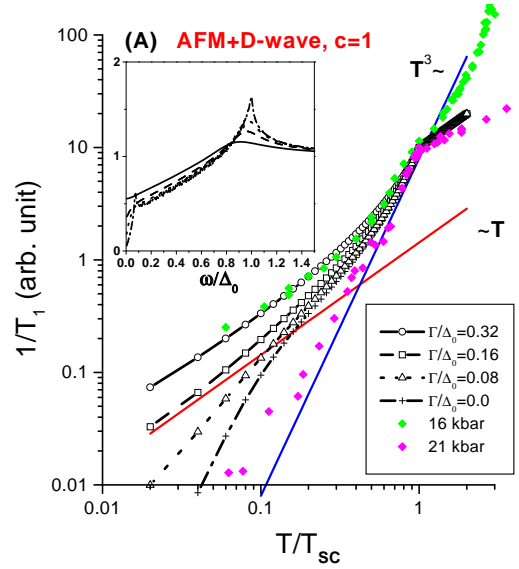
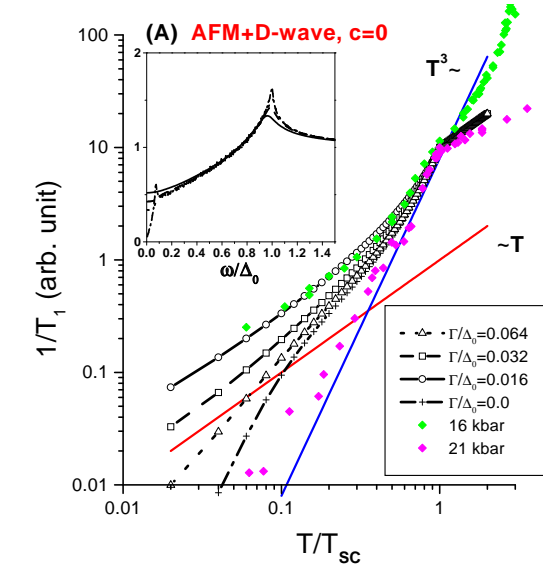


FIG. 3. (A) The normalized $1/T_1$ for AFM+D-wave gap (with the AFM nodal point parameter $\eta=0.3$) for unitary scatterer ($c = 0$) with impurity scattering rates of $\Gamma/\Delta_0 = 0.064, 0.032, 0.016, 0.0$. The green diamonds are the normalized 1.6 GPa experimental data and the magenta diamonds are for 2.1 GPa data of CeRhIn₅^{7,8}. Solid lines for T^3 and T are guides for the eyes. Inset: The corresponding normalized DOS $N(\omega)/N_0$, in decreasing order of $N(\omega = 0)$, with $\Gamma/\Delta_0 = 0.064, 0.032, 0.016, 0.0$. (B) The normalized $1/T_1$ for a standard harmonic D-wave gap for unitary scatterer ($c = 0$) with impurity scattering rates $\Gamma/\Delta_0 = 0.064, 0.032, 0.016, 0.0$. The green and magenta diamonds are the same data as in Fig.3 (A). Inset: The corresponding normalized DOS $N(\omega)/N_0$.

FIG. 4. (A) The normalized $1/T_1$ for AFM+D-wave gap (with the AFM nodal point parameter $\eta=0.3$) for Born scatterer ($c = 1$) with impurity scattering rates of $\Gamma/\Delta_0 = 0.32, 0.16, 0.08, 0.0$. The green diamonds are the normalized 1.6 GPa experimental data and the magenta diamonds are for 2.1 GPa data of CeRhIn₅^{7,8}. Solid lines for T^3 and T are guides for the eyes. Inset: The corresponding normalized DOS $N(\omega)/N_0$, in decreasing order of $N(\omega = 0)$, with $\Gamma/\Delta_0 = 0.32, 0.16, 0.08, 0.0$. (B) The normalized $1/T_1$ for a standard harmonic D-wave gap with Born scatterer ($c = 1$) with impurity scattering rates of $\Gamma/\Delta_0 = 0.32, 0.16, 0.08, 0.0$. The green and magenta diamonds are the same data as in Fig.4 (A). Inset: The corresponding normalized DOS $N(\omega)/N_0$.

- * Permanent address: Department of Physics, Chonnam National University, Kwangju 500-757, Korea.
- ¹ G.R. Stewart, *Rev. Mod. Phys.* **73**, 797 (2001), F. Steglich, P. Gegenwart, C. Geibel, R. Helfrich, P. Hellmann, M. Lang, A. Link, R. Modler, G. Sparn, N. Beuttgen, and A. Loidl, *Physica B* **223-224**, 1 (1996); J. D. Thompson et al., cond-mat/0209115, to be published in LT-23 proceedings (2002).
 - ² Bumsoo Kyung, *Phys. Rev. B* **62**, 9083 (2000); M. Inui, S. Doniach, P.J. Hirschfeld, and A.E. Ruckenstein, *Phys. Rev. B* **37**, 2320 (1988); M. Kato and K. Machida, *Phys. Rev. B* **37**, 1510 (1988).
 - ³ Y. Kawasaki, K. Ishida, T. Mito, C. Thessieu, G.-q. Zheng, and Y. Kitaoka, *Phys. Rev. B* **63**, 140501 (2001).
 - ⁴ Y. Kohori, K. Matsuda, and T. Kohara, *J. Phys. Soc. Japan* **65**, 1083 (1996).
 - ⁵ Y. Kawasaki, K. Ishida, K. Obinata, K. Tabuchi, K. Kashima, and Y. Kitaoka, *Phys. Rev. B* **66**, 224502 (2002).
 - ⁶ H. Tou, Y. Kitaoka, K. Asayama, C. Geibel, C. Schank, and F. Steglich, *J. Phys. Soc. Japan* **64**, 725 (1995).
 - ⁷ S. Kawasaki, T. Mito, G.-q. Zheng, C. Thessieu, Y. Kawasaki, K. Ishida, Y. Kitaoka, T. Muramatsu, T.C. Kobayashi, D. Aoki, S. Araki, Y. Haga, R. Settai, and Y. Onuki, *Phys. Rev. B* **65**, 020504 (2001); S. Kawasaki et al., cond-mat/0303123.
 - ⁸ T. Mito, S. Kawasaki, G.-q. Zheng, Y. Kawasaki, K. Ishida, Y. Kitaoka, D. Aoki, Y. Haga, and Y. Onuki, *Phys. Rev. B* **63**, 220507 (2001).
 - ⁹ A.I. Buzdin and L.H. Bulaevskii, *Sov. Phys. Usp.* **29**, 412 (1986). In this paper the authors consider the case of s-wave SC with AFM long range order. Our work is an extension of their analysis to the D-wave case.
 - ¹⁰ Yunkyu Bang, I. Martin, and A.V. Balatsky, *Phys. Rev. B* **66**, 224501 (2002).
 - ¹¹ P. J. Hirschfeld, P. Woelfle, and D. Einzel, *Phys. Rev. B* **37**, 83 (1988).
 - ¹² The AFM fluctuations mediated D-wave pairing has been mostly studied in the paramagnetic phase. In the AFM ordered phase still the longitudinal mode χ_{\parallel} can mediate the D-wave pairing and has basically the same form as in the paramagnetic phase. The issue of pair breaking and pair mediating by the transverse modes in the AFM phase is beyond the scope of this work.
 - ¹³ Han-Yong Choi, *Phys. Rev. Lett.* **81**, 441 (1998).
 - ¹⁴ R. A. Fisher, F. Bouquet, N. E. Phillips, M. F. Hundley, P. G. Pagliuso, J. L. Sarrao, Z. Fisk, and J. D. Thompson, *Phys. Rev. B* **65**, 224509 (2002).
 - ¹⁵ K. Izawa, H. Yamaguchi, Y. Matsuda, H. Shishido, R. Settai, and Y. Onuki, *Phys. Rev. Lett.* **87**, 057002 (2001).